

DIAGNOSING CLEFT LIP PATHOLOGY IN 3D ULTRASOUND: A LANDMARKING-BASED APPROACH

Original

DIAGNOSING CLEFT LIP PATHOLOGY IN 3D ULTRASOUND: A LANDMARKING-BASED APPROACH / Vezzetti, Enrico; Marcolin, Federica; Fracastoro, Giulia; Speranza, Domenico. - In: IMAGE ANALYSIS & STEREOLOGY. - ISSN 1580-3139. - ELETTRONICO. - 35:1(2016), pp. 53-65. [10.5566/ias.1339]

Availability:

This version is available at: 11583/2625310 since: 2016-10-20T11:34:45Z

Publisher:

international society for Stereology

Published

DOI:10.5566/ias.1339

Terms of use:

This article is made available under terms and conditions as specified in the corresponding bibliographic description in the repository

Publisher copyright

(Article begins on next page)

DIAGNOSING CLEFT LIP PATHOLOGY IN 3D ULTRASOUND: A LANDMARKING-BASED APPROACH

ENRICO VEZZETTI¹, DOMENICO SPERANZA², FEDERICA MARCOLIN¹, AND GIULIA FRACASTORO¹

¹Department of Management and Production Engineering, Politecnico di Torino, Italy;

²Dipartimento di Ingegneria Civile e Meccanica, Università degli Studi di Cassino e del Lazio Meridionale, Italy

e-mails: enrico.vezzetti@polito.it; d.speranza@unicas.it; federica.marcolin@polito.it;

giulia.fracastoro@studenti.polito.it

11

12

13

14

ABSTRACT

16

Aim of this work is to automatically diagnose and formalize prenatal cleft lip with representative key points and identify the type of defect (unilateral, bilateral, right, or left) in three-dimensional ultrasonography (3D US). Differential Geometry has been used as a framework for describing facial shapes and curvatures. Then, descriptors coming from this field are employed for identifying the typical key points of the defect and its dimensions. The descriptive accurateness of these descriptors have allowed us to automatically extract reference points, quantitative distances, labial profiles, and to provide information about facial asymmetry. Eighteen foetal faces, ten of healthy fetuses and eight with different types of cleft lips, have been obtained through a Voluson system and used for testing the algorithm. Cleft lip has been diagnosed and correctly characterized in all cases. Transverse and cranio-caudal length of the cleft have been computed and upper lip profile has been automatically extracted to have a visual quantification of the overall labial defect. The asymmetry information obtained is consistent with the defect. This algorithm has been designed to support practitioners in identifying and classifying cleft lips. The gained results have shown that Differential Geometry might be a proper tool for describing faces and for diagnosis.

34

Keywords: Cleft lip; dysmorphisms; landmarking; syndrome diagnosis; 3D ultrasound.

36

37

38

INTRODUCTION

40

Three-dimensional ultrasound (US) has been introduced more than twenty years ago into clinical practice (Riccabona *et al.*, 1997). Its applications on diagnosis of anomalies and diseases were a direct consequence of its use. In particular, cleft lip and palate (CLP) detection, whose incidence is 1/700 in United States (Tonni and Lituanian, 2013), was widely addressed, as they could be difficult to be diagnosed with bi-dimensional US, especially in earlier gestational ages (Hata *et al.*, 1998). In the effort to quantify the performance of routine ultrasonographic screening on an unselected population, the Eurofetus study (Grandjean *et al.*, 1999) shows that CLP has the lowest rates of detection (18%) and it is diagnosed usually later in pregnancy (only 31.6% before 24 weeks). Furthermore, CLP is identified with a lower occurrence by prenatal US when the anomaly is isolated than in the cases where multiple

52anomalies coexist, as frequently noticed during autopsies following termination of
53pregnancy of fetuses with diagnosed multiple diseases (Luck *et al.*, 1992).
54Complementarily, 3D, despite some criticisms (Maarse *et al.*, 2010), has been
55considered more accurate than bi-dimensional data in detecting unaffected lips at less
56than 24 weeks (Pretorius *et al.*, 1995).

57 In this work we will focus on cleft lip (CL) alone. CL, “both unilateral and
58bilateral, includes clefts involving the alveolus and hard palate anterior to the incisive
59foramen, namely the embryological primary palate” (Demircioglu *et al.*, 2008). The
60tested rates of antenatal detection of CL range 21-30% (Rotten and Levailant, 2004).

61 Cleft lip has been associated with more than one-hundred different
62chromosomal abnormalities and genetic syndromes (Jones, 1993), and sometimes may
63be the only sign of a chromosomal anomaly, as trisomy 18 (Carlson, 2000), trisomy 13,
64or syndromes such as Cornelia de Lange or Smith-Lemli-Opitz (Roelfsema *et al.*, 2007).
65Thus, an accurate scan searching for other foetal anomalies and a genetic counselling
66are paramount when a cleft lip is diagnosed. Cleft lip does not go with any palatal
67abnormality in 15-25% cases (Bäumler *et al.*, 2011, Offerdal *et al.*, 2008). More
68generally, if we consider CLP as a whole, the incidence of structural anomalies and
69syndromes accompanying cleft lip and palate ranges between 21% and 38%
70(Campbell *et al.*, 2005). But it is important to note that, although they often occur with
71each other, cleft lip and palate abnormalities are “developmentally distinct processes”
72(Lee *et al.*, 2000). In particular, the embryological origins of lips and alveolus clefts
73appear to be distinct from those of secondary palate cleft (Campbell *et al.*, 2005).

74 Lee *et al.* (2000) used three-dimensional ultrasonography to support cleft lip
75and palate detection. CL was identified by an examiner as “a loss of continuity of the
76orbicularis oris muscle from a coronal or axial view of the lips” (Lee *et al.*, 2000), so
77the diagnosis was not automatic. Campbell *et al.* (2005) assessed the clinical value of
78a three-dimensional US technique, the 'reverse face' view, in the prenatal
79categorization of orofacial clefts including CL. Then, Platt *et al.* (2006) proposed the
80'flipped face' view to diagnose lip and palate cleftings, relying on 3D US. When a static
81volume is acquired, it is rotated 90° so that the cut plane is directed in a chin-to-nose
82plane and scrolled to examine in sequential order different zones, including lips.
83Mailáth-Pokorny *et al.* (2010) investigated the role of foetal MRI in the antenatal
84diagnosis of facial clefts, including cleft lip, although no particular detection technique
85has been employed. Martinez-Ten *et al.* (2012) investigated whether systematic
86examination of primary and secondary palate supported the detection of face cleftings
87during first trimester. Gindes *et al.* (2013) studied the potential of three-dimensional
88US for palate view in fetuses at high risk for CLP. An in-depth palate assessment was
89made adopting both 2D and 3D US on the axial plane. Then, the outcoming prenatal
90diagnosis was compared to after-birth findings.

91 Some authors used landmarks as reference points. Johnson *et al.* (2000)
92assessed the advantages of three-dimensional US in diagnosing cleft lip. The volume
93data were displayed in two formats: three orthogonal planar images and a three-
94dimensional rendered image of the foetal facial surface. The planar images were
95“rotated with the interactive display into a standard anatomic orientation, so that the
96three planar images corresponded to the frontal, sagittal, and transverse facial planes”
97(Johnson *et al.*, 2000). The rendered image provided landmarks for the planar images.
98Roelfsema *et al.* (2007) used 3D US to perform foetal orofacial clefts examination and
99quantified the craniofacial variability index (CVI) in distinguishing between isolated

cleft lip/palate and cleft lip/palate in chromosomal abnormalities or syndromes. Facial landmarks such as tragus, nasion, gnathion, glabella, subnasion, and others were employed to extract sixteen craniofacial measurements for the evaluation of after-birth abnormal/regular orofacial development. Although none of the fetuses evaluated in their study was affected by cleft lip, Sepulveda *et al.* (2010) proposed a novel sonographic landmark typical of the first trimester, the 'retronasal triangle', to be adopted for the early screening of CP. This landmark has been termed this way because coronal plane displays three easily identifiable echogenic lines: the two maxilla frontal processes and the primary palate. Manganaro *et al.* (2011) studied CLP via MRI and ultrasound, although not 3D. Facial landmarks in the zones of forehead, occiput, orbits, nose, lips, chin, mandible were identified and analyzed for each fetus. Tonni and Lituania (2012) proposed a new three-dimensional sonographic software, the OmniView algorithm, and applied it to unilateral CL, bilateral CLP, and isolated CP. They showed that 3D imaging of the foetal hard and soft palates by OmniView was technically easier than with previously reported 3D techniques. OmniView allowed visualization of all anatomical landmarks of the specific targeted zone, i.e. labia, primary palate, alveolar ridge, posterior palate, uvula, velum, and tongue.

This work introduces a methodology for automatically diagnosing cleft lip and assessing specific information about the detected cleft, such as transverse and cranio-caudal lengths, upper lip outline, and a quantification of facial asymmetry.

MATERIALS AND METHODS

During 2013, 38 3D volumes of 38 fetuses at 22-32 weeks' gestation were acquired. Eight of them were fetuses affected by cleft lip. Written informed consent was obtained from the parents for publication of clinical details, clinical images, and videos. Principles outlined in the Declaration of Helsinki have been followed.

Among these acquisitions, 18 were selected and processed for the purposes of the study, keeping all the eight faces with cleft lip. The leftover ones were excluded due to damages, acquisition inaccuracy, noise, and wrong or unusable fetus's position, such as hands on face or similar.

The US equipment was a Voluson system (GE Healthcare, Wauwatosa, WI, USA), with a RAB 4-8 (real time 4D convex transducer probe). The GE RAB 4-8 has a frequency range of 4 to 8 MHz and is used for OB applications (Footprint 63.6 x 37.8 mm, FOV 70°, V 85°x70°). Table 1 shows data details and respective scan settings.

Ultrasound examination											
Volume Ultrasound: GE Voluson e - Transducer: RAB 4-8-RS/OB											
Foetus		Scan Setting									Defect
Name	Week	MI	Fr	TIs	Quality	Th	B(°)	V(°)	Mix	SR I	Cleft lip?
Anto	32	0,9	4,2/10,8 cm/51 Hz	0,1	max	30	52	65	40/60	II	no
Bart	32	0,9	3,7/11,0 cm/52 Hz	0,1	max	29	50	65	50/50	II	no
Lisa	32	1,	4,1/9,7 cm/54	0,	max	3	53	65	40/6	II	no

		1	Hz	1		0			0		
Gio	22	1, 1	3,6/10,2 cm/58 Hz	0, 1	max	3 0	47	65	40/6 0	II	no
Gian	22	1, 0	3,6/8,1 cm/68 Hz	0, 1	high 2	3 0	46	65	40/6 0	II	no
Paul	32	1, 1	2,8/10,9 cm/49 Hz	0, 2	max	3 0	54	65	40/6 0	II	no
Pie	32	1, 1	1,7/8,1 cm/55 Hz	0, 1	max	3 0	58	65	40/6 0	II	no
Elen a	32	0, 9	4,2/10,8 cm/47 Hz	0, 1	max	3 0	56	65	40/6 0	II	no
Fede	32	0, 9	4,4/11,1 cm/51 Hz	0, 1	max	3 0	50	65	40/6 0	II	no
Simo n	32	1, 1	3,5/9,6 cm/56 Hz	0, 1	max	3 0	50	65	40/6 0	II	no
A	32	0, 9	4,2/10,8 cm/51 Hz	0, 1	max	3 0	52	65	40/6 0	II	Unilateral complete
B	32	0, 9	3,7/11,0 cm/52 Hz	0, 1	max	2 9	50	65	50/5 0	II	Unilateral complete
C	32	0, 9	4,2/10,8 cm/47 Hz	0, 1	max	3 0	56	65	40/6 0	II	Bilateral complete
D	32	0, 9	4,4/11,1 cm/51 Hz	0, 1	max	3 0	50	65	40/6 0	II	Bilateral complete
E	22	1, 0	3,6/8,1 cm/68 Hz	0, 1	high 2	3 0	46	65	40/6 0	II	Unilateral incomplete
F	32	1, 1	4,1/9,7 cm/54 Hz	0, 1	max	3 0	53	65	40/6 0	II	Unilateral incomplete
G	32	1, 1	2,8/10,9 cm/49 Hz	0, 2	max	3 0	54	65	40/6 0	II	Unilateral complete
H	32	1, 1	3,5/9,6 cm/56 Hz	0, 1	max	3 0	50	65	40/6 0	II	Unilateral incomplete

138 **Table 1.** Weeks' gestation, scan settings, and eventual cleft lip features for each baby.

139
140 4D VIEW software allows to see the acquired images on three orthogonal planes: axial,
141 sagittal, and coronal (Fig. 1, above). The plane chosen for the facial shell modelling is
142 the midsagittal (Fig. 1, below).

143

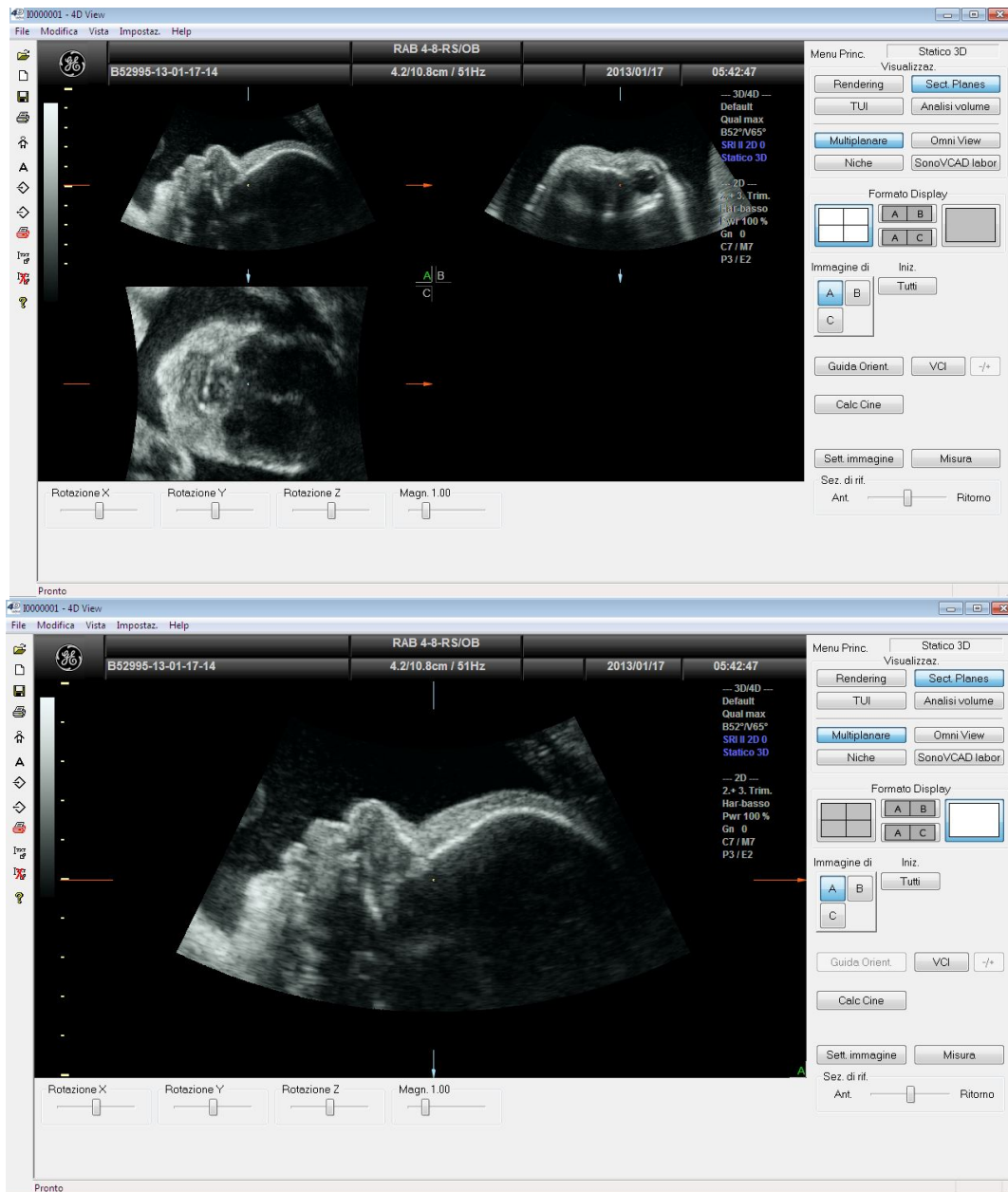


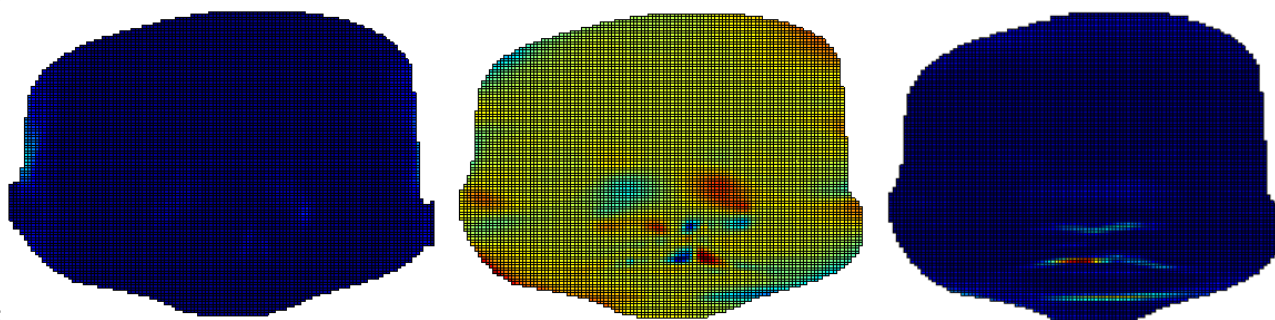
Figure 1. Multiplanar image (above) and midsagittal plane (below).

The distance between two successive slices is 0.4 mm. For each slice composing the whole facial volume, the relative DICOM format file is generated and imported into Simpleware ScanIP software for the three-dimensional model reconstruction. Facial data were collected in point clouds (shells), imported in Matlab®, triangulated, and converted into a squared-grid-based depth map.

The algorithm we developed for foetal diagnosis of cleft lip was elaborated, implemented, and run on these shells. It relies on the geometrical features of foetus's face in order to detect the deformation. Moreover, the algorithm identifies whether the cleft lip is unilateral or bilateral, localizes some key points of the deformation and performs tailored measurements in order to assess cleft quantification. The upper lip outline is also evaluated, in order to provide shape and size description of the defect. The geometrical descriptors used in this work are defined and described in the Appendix. These descriptors rely on previous work of our research group (Calignano

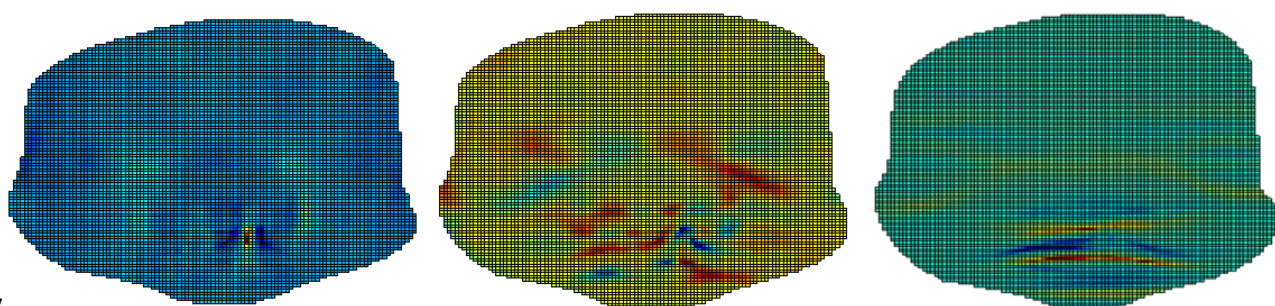
161and Vezzetti, 2010; Vezzetti *et al.*, 2011-2014). Figures 2-8 show their behaviour on a
 162facial shell with cleft lip.

163
 164



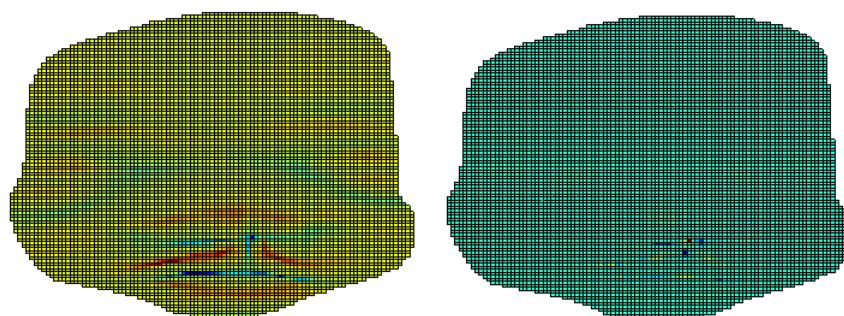
165
 166

Figure 2. The coefficients of the first fundamental form E , F and G .



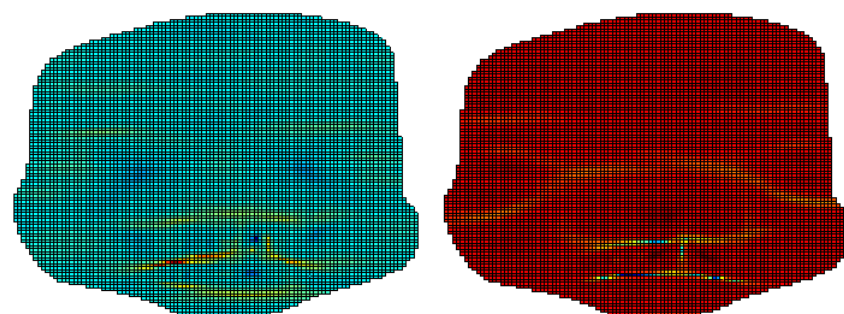
167
 168

Figure 3. The coefficients of the second fundamental form e , f and g .



169
 170

Figure 4. The mean and Gaussian curvature H and K .



171
 172
 173

Figure 5. The principal curvatures k_1 and k_2 .

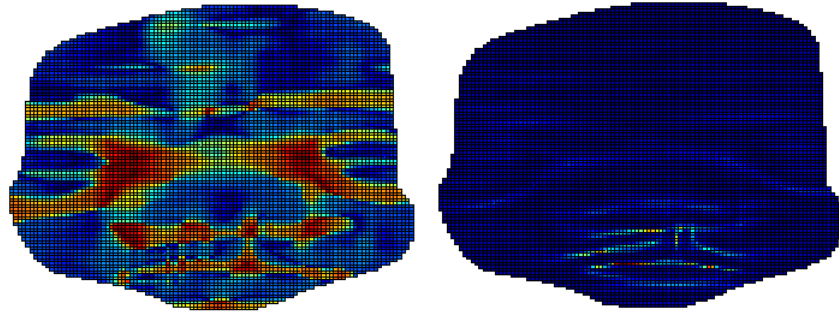


Figure 6. The Shape and Curvature Indexes S and C .

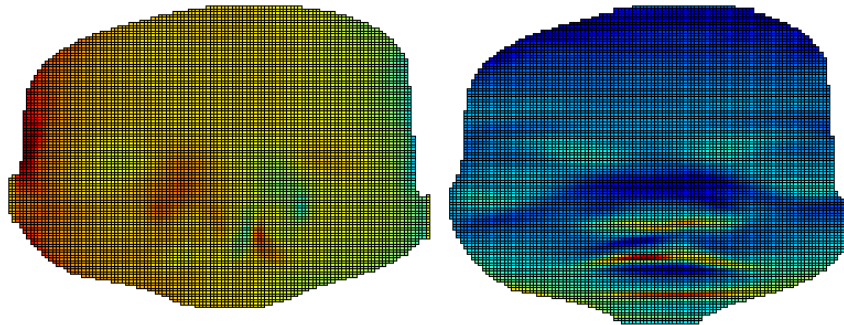


Figure 7. The first derivatives D_x and D_y .

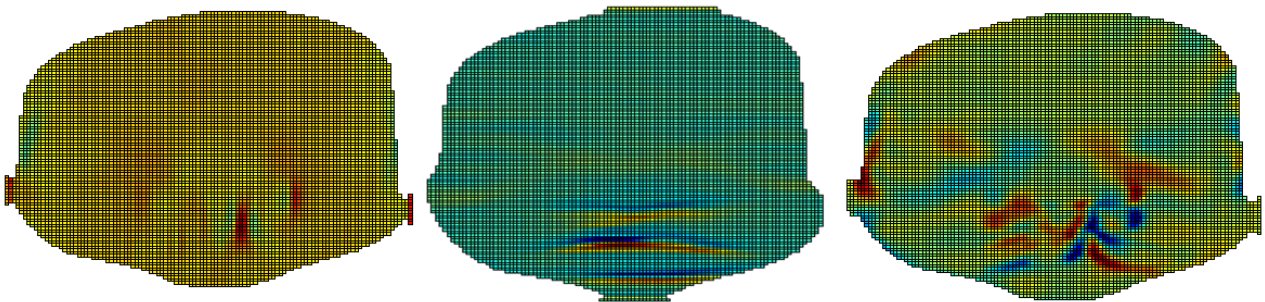
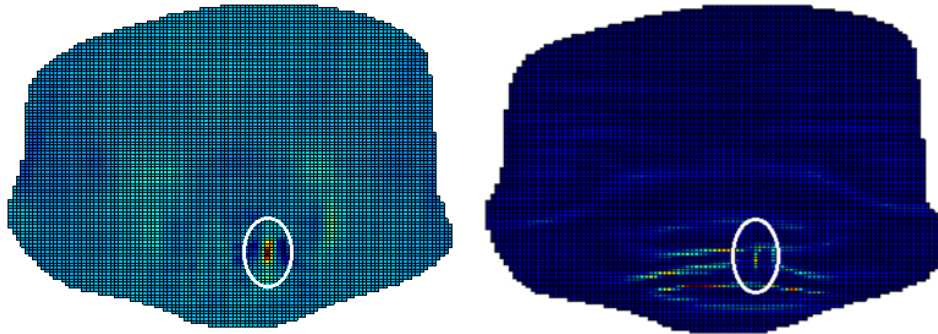


Figure 8. The second derivatives D_{xx} , D_{yy} and D_{xy} .

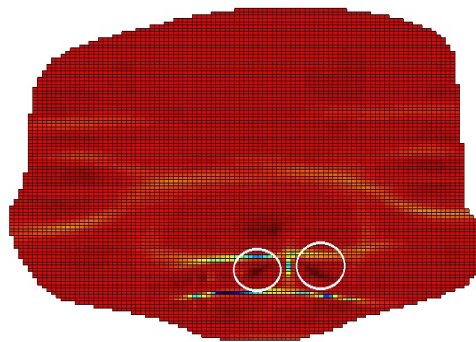
183DETECTION OF THE DEFORMITY

184
185 Cleft lip is a gap/indentation in the upper lip. The proposed algorithm
186demonstrates that this defect could be detected via point-by-point mapping
187geometrical descriptors on facial depth map. This indentation is characterized by high
188numerical values of coefficient e and of Curvedness Index C in correspondence to the
189zone of interest, as shown in Figure 9. Moreover, the two parts of the lip that are
190located beside the indentation are characterized by two maximums of the principal
191curvature k_2 , as can be seen in Figure 10.

192



193
194**Figure 9.** The behaviour of the coefficient e (left) and of the Curvedness Index C (right) in a foetus with
195cleft lip. The circle highlights the area of the gap.



196
197**Figure 10.** The behaviour of the principal curvature k_2 in a foetus with cleft lip. The two circles highlight
198the areas of the lip beside the gap.

199

200 The designed algorithm adopts the previous geometrical features to detect
201whether the cleft lip is present or not in a foetus's face. Moreover, this algorithm is
202able to automatically distinguish between unilateral and bilateral cleft lip. It is
203composed by the following steps.

- 204 1. The algorithm searches if there are points whose coefficient e and Curvedness
205 Index C are greater than a threshold value ($C > 3$ and $e > 3.5$). These are the
206 geometrical features of the gap in the lip. Thresholds are set via
207 experimentation.
- 208 2. If the search of the step 1 gives no results, the cleft lip is not present.
209 Otherwise, another check is performed in order to verify that a cleft lip is really
210 present. For each point that satisfies the conditions of step 1, the algorithm
211 searches if in its neighbourhood there are points with a high value of the
212 principal curvature k_2 ($k_2 > 0.3$). These are the geometrical features of the two
213 parts of the lip beside the gap. This further condition is needed, as in some

- cases the points close to the *a/ae* of the nose could have the same geometrical features searched in step 1.
3. If the search of the previous step gives no results, the cleft lip is not present; otherwise it is.
 4. In order to verify if it is an unilateral or bilateral cleft lip, the algorithm checks if the points that satisfy the condition of step 1 and 2 are all in the same neighbourhood or not. If they do not belong to the same neighbourhood, the cleft lip is bilateral.

The steps of the process are explained in the scheme of Figure 11.

In Figure 12, the points found in step 1 and 2 are shown in a shell with an unilateral cleft lip.

In Figure 13, the points found in step 1 and 2 are shown in a shell with a bilateral cleft lip.

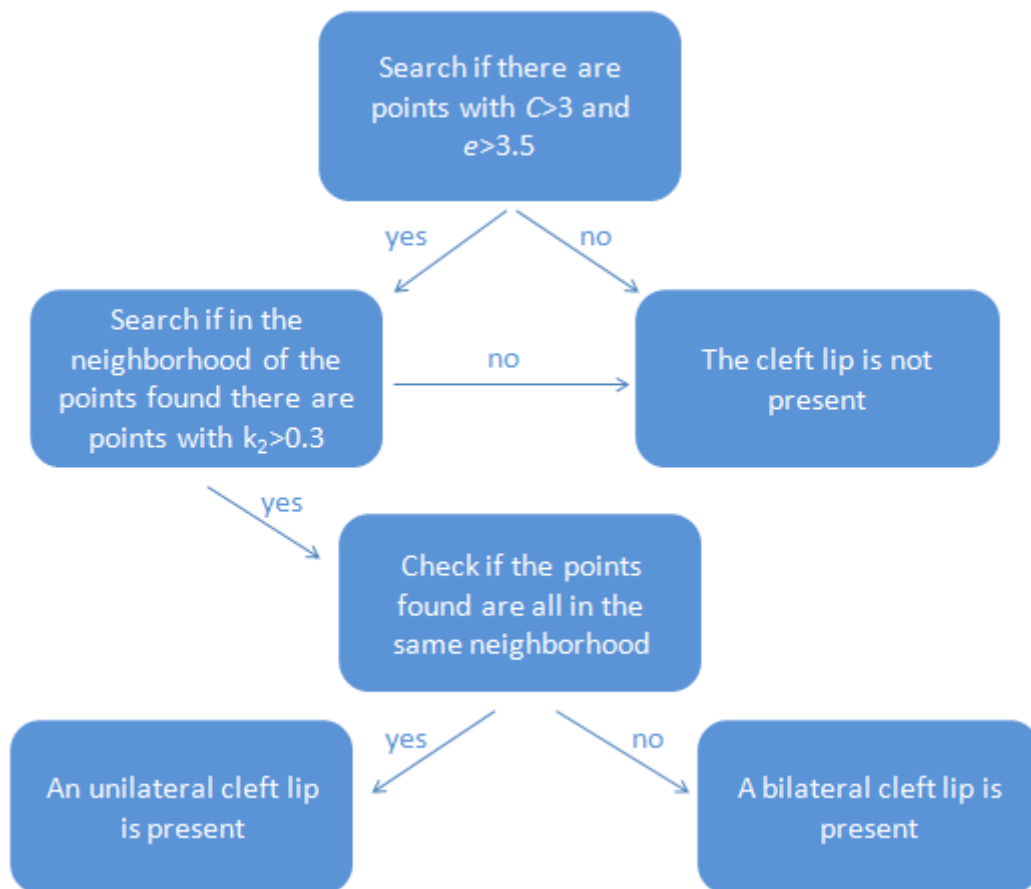
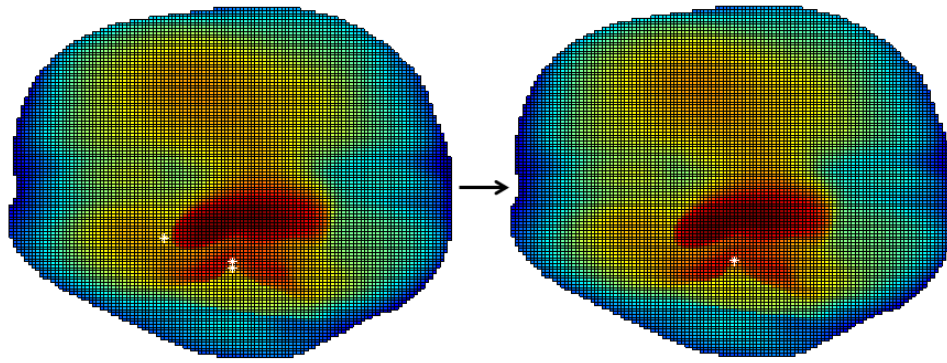
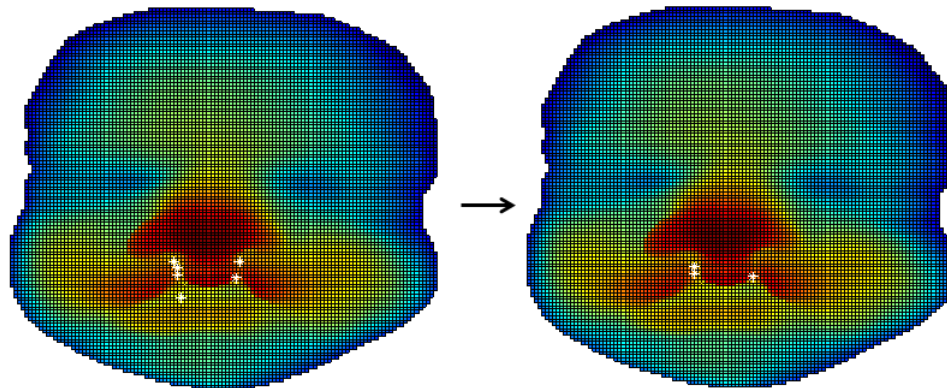


Figure 11. Scheme of the process for cleft lip diagnosis.



230
231 **Figure 12.** On the left: the points found in the first step of the algorithm. On the right: the points found in
232 the second step of the algorithm.



233
234 **Figure 13.** On the left: the points found in the first step of the algorithm. On the right: the points found in
235 the second step of the algorithm.

236

237 LOCALIZATION OF KEY POINTS

238

239 In order to quantify the deformation, four key points are automatically localized:
240 the two points of the lip that are beside the cleft and the ending points of the cleft,
241 shown in Figure 14.

242



Figure 14. The four key points of the cleft lip.

243
244
245

246 As mentioned above, the principal curvature k_2 has two maximums in the first
247 two points. The automatic localization algorithm:

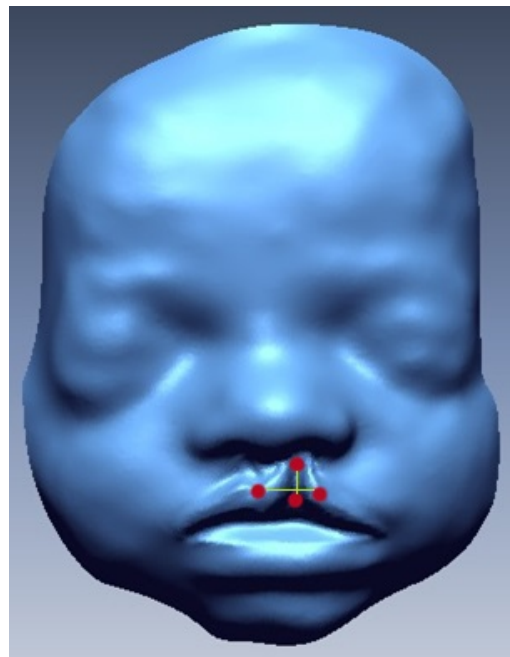
- 248 1. after deformity detection, identifies two regions in the neighbourhood of the
249 cleft, one on the right side and one on the left side;
- 250 2. in each region, selects the points with $D_y < 0$;
- 251 3. maximizes the principal curvature k_2 .

252 The other two points are located in the gap of the lip. As said above, this area is
253 characterized by high values of the Curvedness Index C and of coefficient e . To extract
254 these points, firstly the algorithm localizes the centre of the cleft maximizing the
255 coefficient e . Then, it analyzes the neighbourhood of this point, moving upwards from
256 the centre to the high ending point and downwards till the low ending point. The
257 algorithm, for each y value, maximizes the coefficient e in a neighbourhood of the cleft
258 lip. The ending points are the first two maximums that are lower than a proper
259 threshold value, established via experimentation.

260
261
262 MEASUREMENT OF THE DEFORMATION AND EXTRACTION OF THE UPPER LIP
263 OUTLINE

264
265 Transverse diameter of the cleft was evaluated by computing the Euclidean
266 distance between the first two points extracted; its cranio-caudal length by computing
267 the Euclidean distance between the last two points extracted. These two distances,
268 represented in Figure 15, are the most adopted in the estimation of cleft size.

269



270
271
272

Figure 15. The transverse (horizontal) and cranio-caudal length (vertical) of the cleft.

273 The outline of the upper lip was also extracted, in order to provide an extra
274 information about its shape. The Curvedness Index was adopted, as it is one of the
275 geometrical descriptors that more accurately highlights upper lip surface behaviour. As
276 shown in Figure 16, the Curvedness Index has a maximum behaviour in
277 correspondence to the upper lip. To extract the outline, for each x value in the upper

lip area, the Curvedness Index is maximized. This way, we obtain a sequence of points, namely a line, in the 3D space that describes the upper lip area.

281

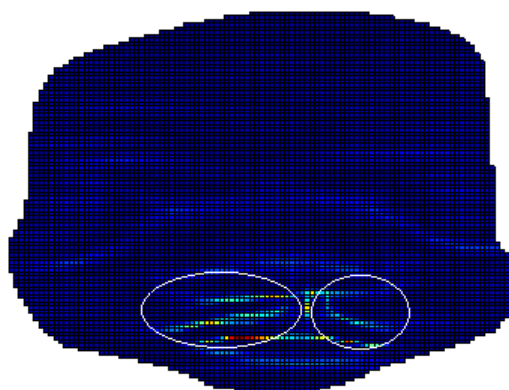


Figure 16. The Curvedness Index. The two circles highlight the upper lip area.

282

283

284

285

286 EVALUATION OF FACE ASYMMETRY

287

288 Facial asymmetry was also evaluated in the cases of unilateral cleft lip. To
289 perform this evaluation, the mean of the absolute value of the coefficient e was
290 computed in both left and right parts of the mouth. By comparing these two mean
291 values, we obtain an useful information about the asymmetry of the face. Coefficient e
292 is chosen and its absolute value is taken, as in correspondence of the cleft lip two
293 minimums and a maximum are present (as it was previously shown in Figure 8); the
294 absolute value will avoid that the minimum and maximum behaviour will annul each
295 other when the mean area is computed.

296

297

298

299 RESULTS AND DISCUSSION

300

301 The algorithm for the diagnosis of cleft lip was tested on the eighteen
302 ultrasounds (eight with cleft lip and ten without). In all these cases, the algorithm
303 correctly detected the presence/absence of the cleft and, in the two shells with
304 bilateral cleft lip, the algorithm detected both the clefts.

305 In the eight ultrasounds with cleft lip, the four key points were localized. In
306 Figure 17 the resulting four key points are shown for each shell.

307

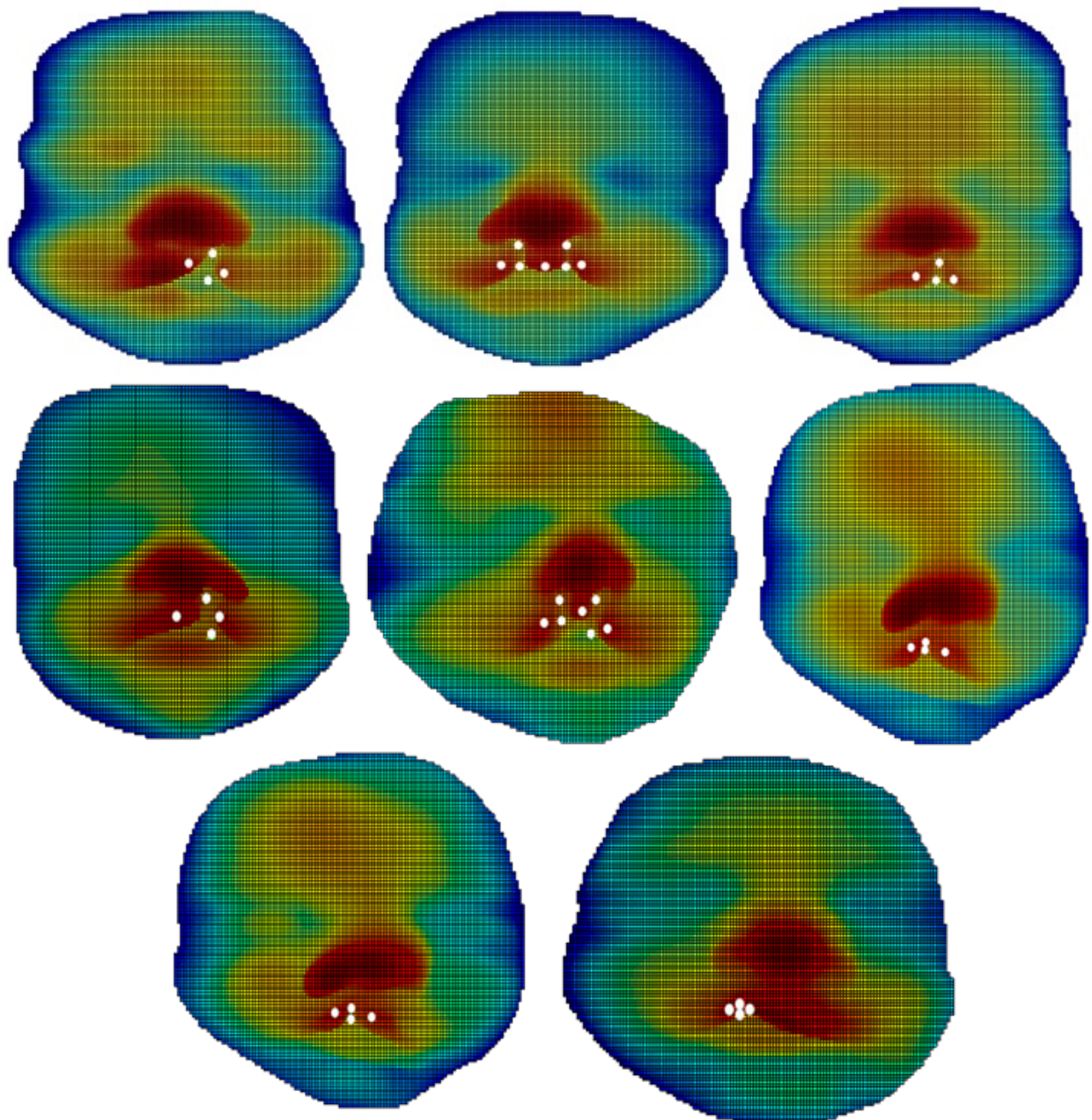


Figure 17. The resulting four key points for each shell with cleft lip.

After having localized the four key points, transverse and the cranio-caudal length are computed. In Table 2, the values of these distances for each shell are shown. The unit of measurement is the millimetre. As can be seen, the shells that present the lowest cranio-caudal length are the ones with an incomplete cleft.

A	7.19	6.78
B	8.31	9.59
C (left cleft)	15.08	7.00
C (right cleft)	12.04	7.06
D (left cleft)	12.65	6.09
D (right cleft)	10.01	12.34

E	6.69	1.81
F	6.67	1.64
G	6.19	4.34
H	3.17	0.62

Table 2. Computed distances for each shell.

For each shell with cleft lip, upper lip outline was extracted. Results are shown in Figure 18.

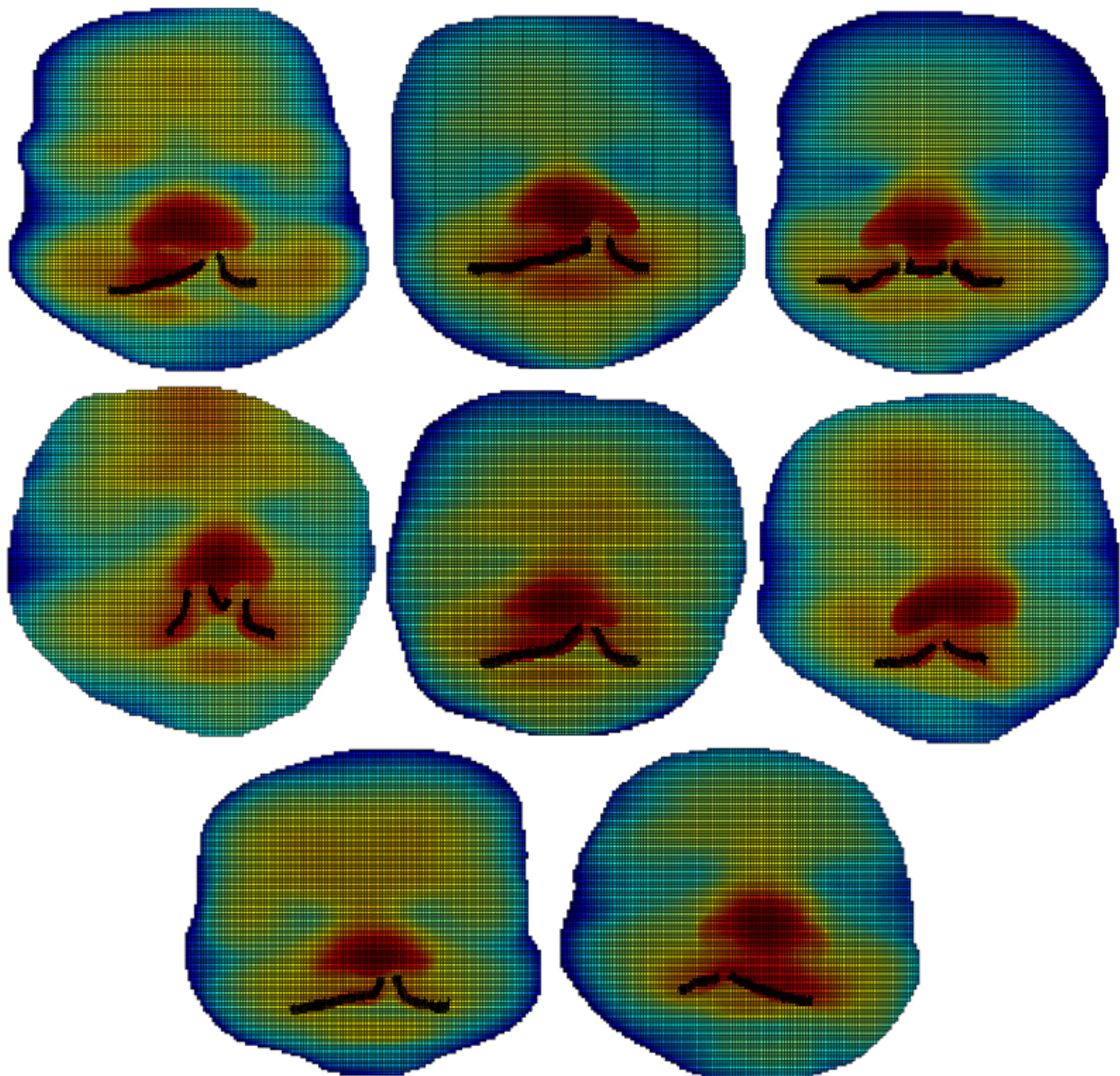


Figure 18. The resulting upper lip outline for each shell with cleft lip.

We computed facial asymmetry in the six shells with unilateral cleft lip and on the ten shells without cleft lip; the evaluation was not performed on the two shells with bilateral cleft lip. The results are shown in Table 3 (shells with unilateral cleft lip) and 4 (shells without cleft lip).

A	1.08	0.41	0.68
B	1.34	0.4	0.94
E	1.10	0.36	0.74
F	0.82	0.60	0.22
G	1.09	0.33	0.76
H	0.44	0.28	0.16

Table 3. Results of asymmetry evaluation for shells with unilateral cleft lip.

Anto	0.28	0.33	0.05
Bart	0.30	0.48	0.18
Elena	0.16	0.27	0.11
Fede	0.33	0.30	0.03
Gian	0.22	0.33	0.11
Gio	0.16	0.24	0.08
Lisa	0.36	0.21	0.14
Paul	0.17	0.22	0.05
Pie	0.15	0.20	0.05
Simon	0.18	0.25	0.07

Table 4. Results of asymmetry evaluation for shells without cleft lip.

As can be seen in Tables 3 and 4, the difference between the two sides of the face is usually higher in the shells with cleft lip. The mean difference value is 0.58 mm in shells with cleft lip instead it is 0.09 mm in shells without cleft lip, i.e. about six times smaller. The shell with cleft lip with the lowest difference value is H, where an incomplete cleft lip is present. Probably in this case the asymmetry was not high because the cleft lip was not accentuated, as can be verified in Table 2, where the shell H has the lowest cranio-caudal length. Also, the other shell with a low difference value, namely shell E, presents an incomplete cleft lip. Instead, in the shells without cleft lip the difference between the two face sides is usually low, with values ranging between 0.05 and 0.18 millimetres. The highest values (Bart and Lisa) are probably due to the quality of the ultrasound.

CONCLUSIONS

This work presents a new algorithm for diagnosing cleft lip on 3D ultrasound. The proposed algorithm was developed with Matlab® and tested on eighteen fetuses' faces (eight with cleft lip and ten healthy). The algorithm automatically states whether the defect is present or not, classifies it (unilateral, bilateral, right, left), extracts four key points, transverse and cranio-caudal length of the cleft, and upper lip outline, and provides information on the facial asymmetry. The defect has been correctly diagnosed and classified for all the fetuses.

Differential Geometry provided us with a set of descriptors leading this research activity. The result is that these descriptors are suitable to describe facial shape and curvedness, allowing an accurate extraction of the interested facial features.

358
359
360

361ACKNOWLEDGEMENT

362

363The authors declare that they have no conflicts of interest to disclose.

364

365

366

367

368REFERENCES

369

370 Bäumler M, Faure JM, Bigorre M, Bäumler-Patris C, Boulot P, Demattei C, Captier
371G (2011). Accuracy of prenatal three-dimensional ultrasound in the diagnosis of cleft
372hard palate when cleft lip is present. *Ultrasound Obstet Gynecol* 38:440-444.

373 Calignano F, Vezzetti E (2010). Soft tissue diagnosis in maxillofacial surgery: a
374preliminary study on three-dimensional face geometrical features-based analysis.
375*Aesthetic plastic surgery* 34(2):200-11.

376 Campbell S, Lees C, Moscoso G, Hall P (2005). Ultrasound antenatal diagnosis of
377cleft palate by a new technique: the 3D 'reverse face' view. *Ultrasound Obstet Gynecol*
37825:12-18.

379 Carlson DE (2000). Opinion — The ultrasound evaluation of cleft lip and
380palate—a clear winner for 3D. *Ultrasound Obstet Gynecol* 16:299-301.

381 Demircioglu M, Kangesu L, Ismail A, Lake E, Hughes J, Wright S, Sommerlad BC
382(2008). Increasing accuracy of antenatal ultrasound diagnosis of cleft lip with or
383without cleft palate, in cases referred to the North Thames London Region. *Ultrasound*
384*Obstet Gynecol* 31:647-51.

385 Gindes I, Weissmann-Brenner A, Zajicek M, Weisz B, Shrim A, Geffen KT, Mendes
386D, Kuint J, Berkenstadt M, Achiron R (2013). Three-dimensional ultrasound
387demonstration of the fetal palate in high-risk patients: the accuracy of prenatal
388visualization. *Prenatal Diagnosis* 33:436-41.

389 Grandjean H, Larroque D, Levi S (1999). The performance of routine
390ultrasonographic screening of pregnancies in the Eurofetus Study. *Am J Obstet*
391*Gynecol* 181(2):446-54.

392 Hata T, Yonehara T, Aoki S, Manabe A, Hata K, Miyazaki K (1998). Three-
393Dimensional Sonographic Visualization of the Fetal Face. *American Journal of*
394*Roentgenology* 170(February):481-3.

395 Luck CA (1992). Value of routine ultrasound scanning at 19 weeks: a four year
396study of 8849 deliveries. *BMJ* 304(6840):1474-8.

397 Johnson DD, Pretorius DH, Budorick NE, Jones MC, Lou KV, James GM, Nelson TR
398(2000). Fetal Lip and Primary Palate: Three-dimensional versus Two-dimensional US.
399*Radiology* 217(1):236-9.

400 Jones MC (1993). Facial clefting. Etiology and developmental pathogenesis. *Clin*
401*Plast Surg* 20(4):599-606.

402 Lee W, Kirk JS, Shaheen KW, Romero R, Hodges AN, Comstock CH (2000). Fetal
403cleft lip and palate detection by three-dimensional ultrasonography. *Ultrasound Obstet*
404*Gynecol* 16:314-20.

405 Maarse W, Bergé SJ, Pistorius L, Van Barneveld T, Kon M, Breugem C, Mink van
406der Molen AB (2010). Diagnostic accuracy of transabdominal ultrasound in detecting
407prenatal cleft lip and palate: a systematic review. *Ultrasound Obstet Gynecol* 35:495-
408502.

409 Mailáth-Pokorny M, Worda C, Krampl-Bettelheim E, Watzinger F, Brugger PC,
410 Prayers D (2010). What does magnetic resonance imaging add to the prenatal
411 ultrasound diagnosis of facial clefts?. *Ultrasound Obstet Gynecol* 36:445-51.

412 Manganaro L, Tomei A, Fierro F, Di Maurizio M, Sollazzo P, Sergi ME, Vinci V,
413 Bernardo S, Irimia D, Cascone P, Marini M (2011). Fetal MRI as a complement to US in
414 the evaluation of cleft lip and palate. *Radiol med* 116:1134-48.

415 Martinez-Ten P, Adiego B, Illescas T, Bermejo C, Wong AE, Sepulveda W (2012).
416 First-trimester diagnosis of cleft lip and palate using three-dimensional ultrasound.
417 *Ultrasound Obstet Gynecol* 40:40-6.

418 Mittermayer C, Lee A (2003). Picture of the Month — Three-dimensional
419 ultrasonographic imaging of cleft lip: the winners are the parents. *Ultrasound in*
420 *Obstetrics and Gynecology* 21:628-9.

421 Offerdal K, Jebens N, Syvertsen T, Blaas HG, Johansen OJ, Eik-Nes SH (2008).
422 Prenatal ultrasound detection of facial clefts: a prospective study of 49,314 deliveries
423 in a non-selected population in Norway. *Ultrasound Obstet Gynecol* 31(6):639-46.

424 Platt LD, DeVore GR, Pretorius DH (2006). Improving Cleft Palate/Cleft Lip
425 Antenatal Diagnosis by 3-Dimensional Sonography — The “Flipped Face” View. *J*
426 *Ultrasound Med* 25:1423-30.

427 Pretorius DH, House M, Nelson TR, Hollenbach KA (1995). Evaluation of Normal
428 and Abnormal Lips in Fetuses: Comparison Between Three- and Two-Dimensional
429 Sonography. *American Journal of Roentgenology* 165(5):1233-7.

430 Riccabona M, Pretorius DH, Nelson TR, Johnson D, Budorick NE (1997). Three-
431 Dimensional Ultrasound: Display Modalities in Obstetrics. *J Clin Ultrasound* 25(4):157-
432 67.

433 Roelfsema NM, Hop WCJ, Van Adrichem LNA, Wladimiroff JW (2007). Craniofacial
434 variability index determined by three-dimensional ultrasound in isolated vs. syndromal
435 fetal cleft lip/palate. *Ultrasound Obstet Gynecol* 29:265-70.

436 Rotten D, Levailant JM (2004). Two- and three-dimensional sonographic
437 assessment of the fetal face. 1. A systematic analysis of the normal face. *Ultrasound*
438 *Obstet Gynecol* 23:224-31.

439 Sepulveda W, Wong AE, Martinez-Ten P, Perez-Pedregosa J (2010). Retronasal
440 triangle: a sonographic landmark for the screening of cleft palate in the first trimester.
441 *Ultrasound Obstet Gynecol* 35:7-13.

442 Tonni G, Lituania M (2012). OmniView Algorithm — A Novel 3-Dimensional
443 Sonographic Technique in the Study of the Fetal Hard and Soft Palates. *J Ultrasound*
444 *Med* 31:313-8.

445 Tonni G, Lituania M (2013). Arthrogryposis multiplex congenita-like syndrome
446 associated with median cleft lip and palates: First prenatally detected case. *Congenital*
447 *Anomalies* 53:13-40.

448 Vezzetti E, Marcolin F (2012). 3D human face description: landmarks measures
449 and geometrical features. *Image and Vision Computing* 30(10):698-712.

450 Vezzetti E, Marcolin F (2012). Geometrical descriptors for human face
451 morphological analysis and recognition. *Robotics and Autonomous Systems* 60(6):928-
452 39.

453 Vezzetti E, Marcolin F (2012). Geometry-based 3D face morphology analysis:
454 soft-tissue landmark formalization. *Multimedia Tools and Applications* 68(3):895-929.

455 Vezzetti E, Marcolin F (2014). 3D Landmarking in Multiexpression Face Analysis:
456 A Preliminary Study on Eyebrows and Mouth. *Aesthetic Plastic Surgery* 38(4):796-811.

457 Vezzetti E, Calignano F, Moos S (2010). Computer-aided morphological analysis
458for maxillo-facial diagnostic: a preliminary study. *Journal of Plastic, Reconstructive &*
459*Aesthetic Surgery* 63(2):218-26.

460 Vezzetti E, Marcolin F, Fracastoro G (2014). 3D face recognition: An automatic
461strategy based on geometrical descriptors and landmarks. *Robotics and Autonomous*
462*Systems* 62(12):1768-76.

463 Vezzetti E, Marcolin F, Stola V (2013). 3D Human Face Soft Tissues Landmarking
464Method: An Advanced Approach. *Computers in Industry* 64(9):1326-54.

465 Vezzetti E, Moos S, Marcolin F (2011). Three-Dimensional Human Face Analysis:
466Soft Tissue Morphometry. *Proceedings of the InterSymp 2011. Baden-Baden, Germany.*

467 Vezzetti E, Moos S, Marcolin F, Stola V (2012). A pose-independent method for
4683D face landmark formalization. *Computer Methods and Programs in Biomedicine*
469198(3):1078-96.

470 Vezzetti E, Speranza D, Marcolin F, Fracastoro G (2014). Exploiting 3D
471Ultrasound for Fetal Diagnosis Purpose through Facial Landmarking. *Image Analysis &*
472*Stereology* 33(3):167-88.

473

474

475APPENDIX

476

477The First and Second Fundamental Forms are used to measure distance on surfaces
478and are defined by

479

$$480 \quad Edu^2 + 2Fdudv + Gdv^2, \quad (1)$$

481

$$482 \quad ed u^2 + 2fdudv + gdv^2, \quad (2)$$

483

484respectively, where E, F, G, e, f and g are their Coefficients. Curvatures are used to
485measure how a regular surface x bends in R^3 . If D is the differential and N is the
486normal plane of a surface, then the determinant of DN is the product
487 $(-k_1)(-k_2) = k_1 k_2$ of the Principal Curvatures, and the trace of DN is the negative

488 $-(k_1 + k_2)$ of the sum of Principal Curvatures. In point P , the determinant of DN_P is
489the *Gaussian Curvature* K of x at P . The negative of half of the trace of DN is called the
490*Mean Curvature* H of x at P . In terms of the principal curvatures can be written

491

$$492 \quad K = k_1 k_2, \quad (3)$$

493

$$494 \quad H = \frac{k_1 + k_2}{2}.$$

$$495 \quad (4)$$

496

497Some definitions of these descriptors are given. These are the forms implemented in
498the algorithm:

$$499 \quad E = 1 + h_x^2, \quad (5)$$

$$501 \quad F = h_x h_y, \quad (6)$$

$$503 \quad G = 1 + h_y^2, \quad (7)$$

$$505 \quad e = \frac{h_{xx}}{\sqrt{1 + h_x^2 + h_y^2}},$$

$$507 \quad (8)$$

$$508 \quad f = \frac{-h_{xy}}{\sqrt{1 + h_x^2 + h_y^2}},$$

$$510 \quad (9)$$

$$511 \quad g = \frac{-h_{yy}}{\sqrt{1 + h_x^2 + h_y^2}},$$

$$513 \quad (10)$$

$$514 \quad K = \frac{h_{xx} h_{yy} - h_{xy}^2}{(1 + h_x^2 + h_y^2)^2},$$

$$516 \quad (11)$$

$$517 \quad H = \frac{(1 + h_x^2) h_{yy} - 2 h_x h_y h_{xy} + (1 + h_y^2) h_{xx}}{(1 + h_x^2 + h_y^2)^{3/2}},$$

$$519 \quad (12)$$

$$520 \quad k_1 = H + \sqrt{H^2 - K},$$

$$522 \quad (13)$$

$$523 \quad k_2 = H - \sqrt{H^2 - K},$$

$$525 \quad (14)$$

526

527where h is a differentiable function $z=h(x,y)$. It is, therefore, convenient to have at
 528hand formulas for the relevant concepts in this case. To obtain such formulas let us
 529parametrize the surface by

530

$$531 \quad x(u,v)=(u,v,h(u,v)) \quad , \quad (u,v) \in U \quad ,$$

$$532 \quad (15)$$

533

534where $u = x, v = y$.

535

536The most used descriptors are surely the Shape and Curvedness Indexes S and C ,
 537introduced by Koenderink *et al.*¹:

538

$$539 \quad S = \frac{-2}{\pi} \arctan \frac{k_1+k_2}{k_1-k_2} \quad , \quad S \in [-1,1] \quad , \quad k_1 \geq k_2 \quad ,$$

$$540 \quad (16)$$

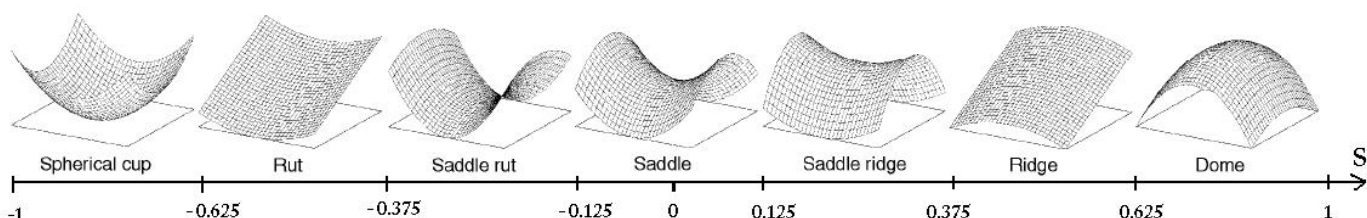
541

$$542 \quad C = \sqrt{\frac{k_1^2+k_2^2}{2}} \quad .$$

$$543 \quad (17)$$

544

545For the role they play in the work, a little digression about their significance is needed.
 546Their meaning is shown in Figures 19-21 and in Table 5.



547

548**Figure 19.** Illustration of Shape Index scale divided into seven categories. Different
 549subintervals of its range $[-1,1]$ correspond to seven geometric surfaces.

550

Class	S	Type	H	K
cup/pit	$[-1,-0.625)$	elliptical convex	+	+
rut/valley	$[-0.625,-0.375)$	cylindrical convex	+	0
saddle rut/saddle valley	$[-0.375,-0.125)$	hyperbolic convex	+	-
saddle	$[-0.125,0.125)$	hyperbolic symmetric	0	-
saddle ridge	$[0.125,0.375)$	hyperbolic concave	-	-
ridge	$[0.375,0.625)$	cylindrical concave	-	0
dome/peak	$[0.625,1)$	elliptical concave	-	+

551

Table 5. Topographic classes.

552

431 Koenderink, J.J. and van Doorn, A.J., 1992. Surface shape and curvature scales.
 44Image and Vision Computing 10(8), 557-564.

45

46



Figure 20. Curvedness Index scale, whose range is $(-\infty, \infty)$.

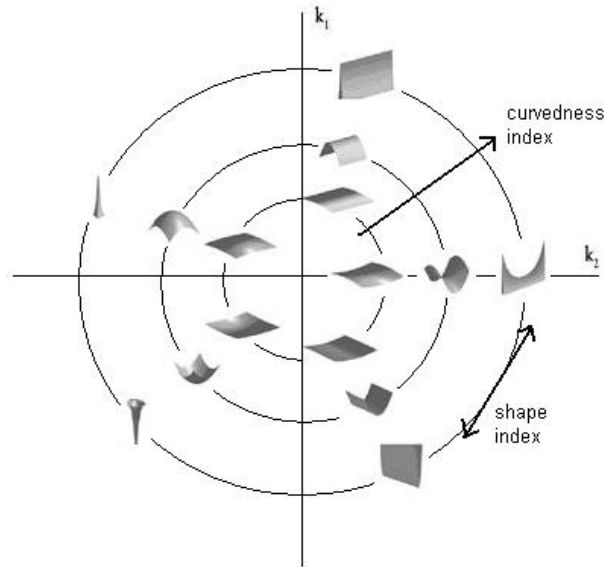


Figure 21. Indexes (S, C) are viewed as polar coordinates in the (k_1, k_2) -plane, with planar points mapped to the origin. The effects on surface structure from variations in the curvedness (radial coordinate) and Shape Index (angular coordinate) parameters of curvature, and the relation of these components to the principal curvatures (k_1 and k_2). The degree of curvature increases radially from the centre.